Lethally Hot Temperatures During the Early Triassic Greenhouse

Yadong Sun *et al.*

Science **338**, 366 (2012);
DOI: 10.1126/science.1224126

Science (print ISSN 0036-8075; online ISSN 1095-9203) is published weekly, except the last week in December, by the American Association for the Advancement of Science, 1200 New York Avenue NW, Washington, DC 20005.

10. L. Marrucci, C. Manzo, D. Paparo, *Phys. Rev. Lett.* **96**, 163905 (2006).
11. G. Biener, A. Niv, V. Kleiner, E. Hasman, *Opt. Lett.* **27**, 1875 (2002).
12. N. Yu *et al.*, *Science* **334**, 333 (2011).
13. M. Smit, J. van der Tol, M. Hill, *Laser Photon. Rev.* **6**, 1 (2012).
14. C. R. Doerr, L. L. Buhl, *Opt. Lett.* **36**, 1209 (2011).
15. K. J. Vahala, *Nature* **424**, 839 (2003).
16. Materials and methods are available as supplementary materials on *Science* Online.
17. A. B. Matsko, A. A. Savchenkov, D. Strekalov, L. Maleki, *Phys. Rev. Lett.* **95**, 143904 (2005).
18. D. Taillaert *et al.*, *Jpn. J. Appl. Phys.* **45**, 6071 (2006).
19. R. Dorn, S. Quabis, G. Leuchs, *Phys. Rev. Lett.* **91**, 233901 (2003).
20. Z. Bomzon, V. Kleiner, E. Hasman, *Opt. Lett.* **26**, 1424 (2001).
21. A. Niv, G. Biener, V. Kleiner, E. Hasman, *Opt. Express* **14**, 4208 (2006).
22. I. Moreno, J. A. Davis, I. Ruiz, D. M. Cottrell, *Opt. Express* **18**, 7173 (2010).
23. A. Yariv, *Electron. Lett.* **36**, 321 (2000).
24. Y. Yu, R. O'Dowd, *IEEE Photon. Technol. Lett.* **14**, 1397 (1992).
25. S. Manipatruni, Q. Xu, M. Lipson, *Opt. Express* **15**, 13035 (2007).
26. K. Ladavac, D. Grier, *Opt. Express* **12**, 1144 (2004).

Acknowledgments: We thank M. Berry and M. Dennis (Department of Physics, University of Bristol, UK), S. Barnett (Department of Physics, University of Strathclyde, UK), and M. Padgett (Department of Physics, University of Glasgow, UK) for very useful discussions and C. Railton (Merchant Venturers School of Engineering, University of Bristol, UK) for providing the finite-difference time-domain simulation tool. J.W. is funded by European Union FP7 FET-OPEN project PHORBITEC.

Supplementary Materials
www.sciencemag.org/cgi/content/full/338/6105/363/DC1
Materials and Methods
Supplementary Text
Figs. S1 to S7
References (*27*–*31*)
Movies S1 to S4

25 June 2012; accepted 10 September 2012
10.1126/science.1226528

Lethally Hot Temperatures During the Early Triassic Greenhouse

Yadong Sun,[1,2]* Michael M. Joachimski,[3] Paul B. Wignall,[2] Chunbo Yan,[1] Yanlong Chen,[4] Haishui Jiang,[1] Lina Wang,[1] Xulong Lai[1]

Global warming is widely regarded to have played a contributing role in numerous past biotic crises. Here, we show that the end-Permian mass extinction coincided with a rapid temperature rise to exceptionally high values in the Early Triassic that were inimical to life in equatorial latitudes and suppressed ecosystem recovery. This was manifested in the loss of calcareous algae, the near-absence of fish in equatorial Tethys, and the dominance of small taxa of invertebrates during the thermal maxima. High temperatures drove most Early Triassic plants and animals out of equatorial terrestrial ecosystems and probably were a major cause of the end-Smithian crisis.

Anthropogenic global warming likely is contributing to the rapid loss of biological diversity currently occurring (*1*). Climate warming also has been implicated in severe biotic crises in the geological past, but only as a corollary to more direct causes of death such as the spread of marine anoxia (*2*). Here, we show that lethally hot temperatures exerted a direct control on extinction and recovery during and in the aftermath of the end-Permian mass extinction. As well as the scale of the losses, the aftermath of this event is remarkable for several reasons, such as the prolonged delay in recovery (*3*), the prevalence of small taxa (*4*), and the absence of coal deposits throughout the Early Triassic (*5*). These and several facets of low-latitude fossil records shown below, including fish, marine reptile, and tetrapod distributions, can be related to extreme temperatures in excess of tolerable thermal thresholds.

Climate warming long has been implicated as one cause of the end-Permian crisis (*2*, *6*), with carbon dioxide release from Siberian eruptions and related processes providing a potential trigger for it (*7*, *8*). Conodont apatite oxygen isotope

[1]State Key Laboratory of Geobiology and Environmental Geology, China University of Geosciences (Wuhan), Wuhan 430074, People's Republic of China. [2]School of Earth and Environment, University of Leeds, Leeds LS2 9JT, UK. [3]GeoZentrum Nordbayern, Universität Erlangen-Nürnberg, Schlossgarten 5, 91054 Erlangen, Germany. [4]Institute of Earth Sciences–Geology and Paleontology, University of Graz, Heinrichstrasse 26, A-8010 Graz, Austria.

*To whom correspondence should be addressed. E-mail: eeys@leeds.ac.uk

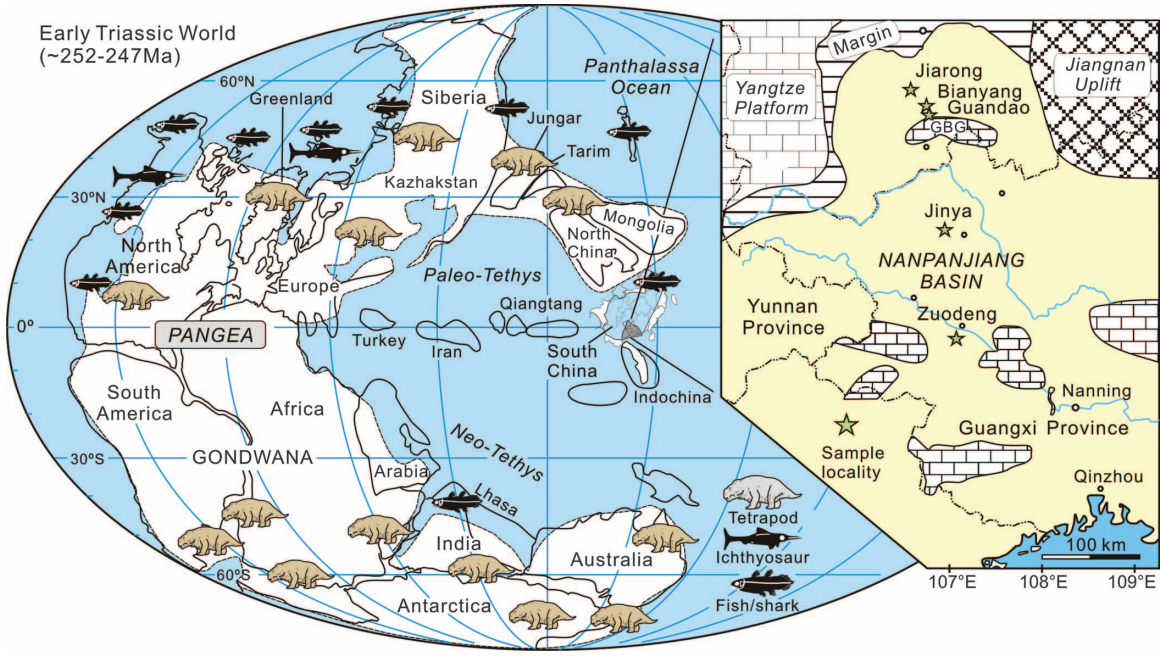

Fig. 1. Early Triassic paleogeography showing reported occurrences of fish and marine reptiles in the Smithian. Note rare equatorial occurrence of both groups when ichthyosaurs had evolved in northern climes. The global distribution of tetrapods (*25*) indicates occurrences almost exclusively in higher latitudes (>30°N and >40°S) throughout the Early Triassic, with rare exceptions in Utah (*Parotosuchus* sp., paleolatitude ~10°N) and Poland (paleolatitude ~20°N), both probably of middle-late Spathian age (*25*, *26*). (**Inset**) Paleogeography of Pangea and Nanpanjiang Basin after (*45*–*47*). Fish and ichthyosaurs occurrences, see table S2. GBG, Great Bank of Guizhou.

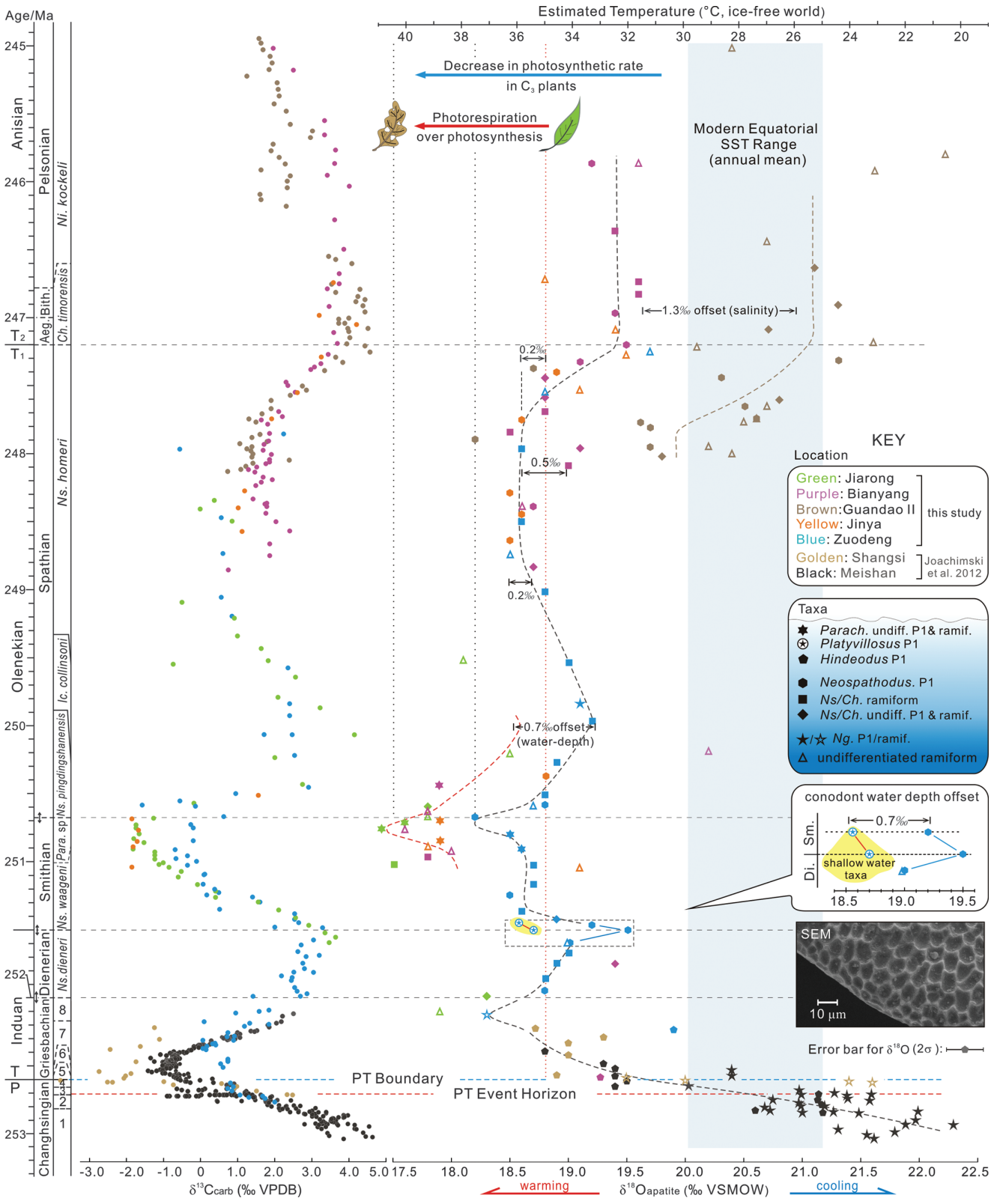

Fig. 2. Oxygen isotopes of conodont apatite and carbon isotopes of carbonates from the Nanpanjiang Basin. Oxygen isotopes show two thermal maxima in the late Griesbachian and late Smithian. Scanning electron microscope investigation of conodont surfaces shows microreticulation and no sign of recrystallization (supplementary text 3). Absolute age constraints are given in supplementary text 9; data for Meishan and Shangsi sections compiled from (*9*); leaf icons represent marine and terrestrial C_3 plants (*14*). Modern equatorial SST ranges (annual mean) from (*48*). The error bar stands for external reproducibility of $\delta^{18}O_{apatite}$ measurements (2σ). The black trendline represents smoothed $\delta^{18}O_{apatite}$ fluctuations estimated from the upper water column taxa. Note uncertainty of correlating conodont zones with absolute ages. Aeg., Aegean; Bith., Bithynian. Conodont zonations: 1, *Ng. changxingensis*; 2, *Ng. yini*; 3, *Ng. meishanensis*; 4, *H. changxingensis*; 5, *H. parvus*; 6, *Is. staeschei*; 7, *Is. isarcica*; 8, *Ng. planata*; for genera abbreviations, see table S4.VSMOW, Vienna Standard Mean Ocean Water; VPDB, Vienna Pee Dee Belemnite.

ratio ($\delta^{18}O$) is a reliable proxy for paleoseawater temperatures (*9*), and conodonts suffered few genus-level losses at the end of the Permian (*10*), allowing continuous sampling of the same genera over multimillion-year intervals (*11*). We used $\delta^{18}O_{apatite}$ of conodonts from sections in the Nanpanjiang Basin, South China, to reconstruct Late Permian to Middle Triassic equatorial seawater temperatures (Fig. 1 and supplementary text 1). Our main record, measured on the genus *Neospathodus*, is a monitor of upper water column temperatures (estimated ~70 m water depth, supplementary text 2), whereas data from extremely shallow water taxa (*Pachycladina* or *Parachirognathus* spp., *Platyvillosus* spp.) provide sea surface temperatures (SSTs).

Our results show large, near-synchronous perturbations in both carbon isotope ratios ($\delta^{13}C_{carb}$) and $\delta^{18}O_{apatite}$ with three positive excursions observed in the Dienerian [~251.5 million years ago (Ma)], early Spathian (~250.5 Ma), and at the Spathian-Anisian (Early-Middle Triassic) transition (~247.5 Ma). The minima in $\delta^{13}C_{carb}$ and $\delta^{18}O_{apatite}$ are measured in the Griesbachian (~252.1 Ma) and the Smithian-Spathian transition (~250.7 Ma) (Fig. 2). The $\delta^{18}O_{apatite}$ values of the analyzed conodonts taxa accord with their habitats in different water depth: *Neospathodus* spp. shows ~0.7 per mil (‰) heavier values than those from shallow-water *Pachycladina*/*Parachirognathus* spp. and *Platyvillosus* spp. Deeper-water gondolellids show even heavier $\delta^{18}O_{apatite}$ (~0.4‰) than *Neospathodus* spp. (supplementary text 2 and table S1). Latest Spathian–early Anisian oxygen isotope data from Bianyang and Guandao are more scattered and up to 1.3‰ heavier compared with samples from other sections. These two locations are close to the Great Bank of Guizhou (Fig. 1), and such ^{18}O enrichment toward platform interior is interpreted to be due to evaporation as seen on the modern Bahama Bank (*12*). However, most of the presented data are from distal, open-water environments and therefore present a faithful paleotemperature record (supplementary texts 3 and 4).

Calculation of seawater temperatures from $\delta^{18}O$ values (supplementary text 5) reveals rapid warming across the Permian-Triassic boundary [21° to 36°C, over ~0.8 million years (My); (*9*)], reaching a temperature maximum within the Griesbachian (~252.1 Ma) followed by cooling in the Dienerian. A second rise to high temperatures is seen in the late Smithian (~250.7 Ma), followed by relatively stable temperatures in the Spathian, cooling at the end of this stage and stabilization in the early Middle Triassic (Fig. 2). The late Smithian Thermal Maximum (LSTM) marks the hottest interval of entire Early Triassic, when upper water column temperatures approached 38°C with SSTs possibly exceeding 40°C (Fig. 3).

The entire Early Triassic record shows temperatures consistently in excess of modern equatorial annual SSTs. These results suggest that equatorial temperatures may have exceeded a tolerable threshold both in the oceans and on land. For C_3 plants, photorespiration predominates over photosynthesis at temperatures in excess of 35°C (*13*), and few plants can survive temperatures persistently above 40°C (*14*). Similarly, for animals, temperatures in excess of 45°C cause protein damage that are only temporarily alleviated by heat-shock protein production (*15*). However, for most marine animals, the critical temperature is much lower, because metabolic oxygen demand increases with temperature while dissolved oxygen decreases (*16*). This causes hypoxaemia and the onset of anaerobic mitochondrial metabolism that is only

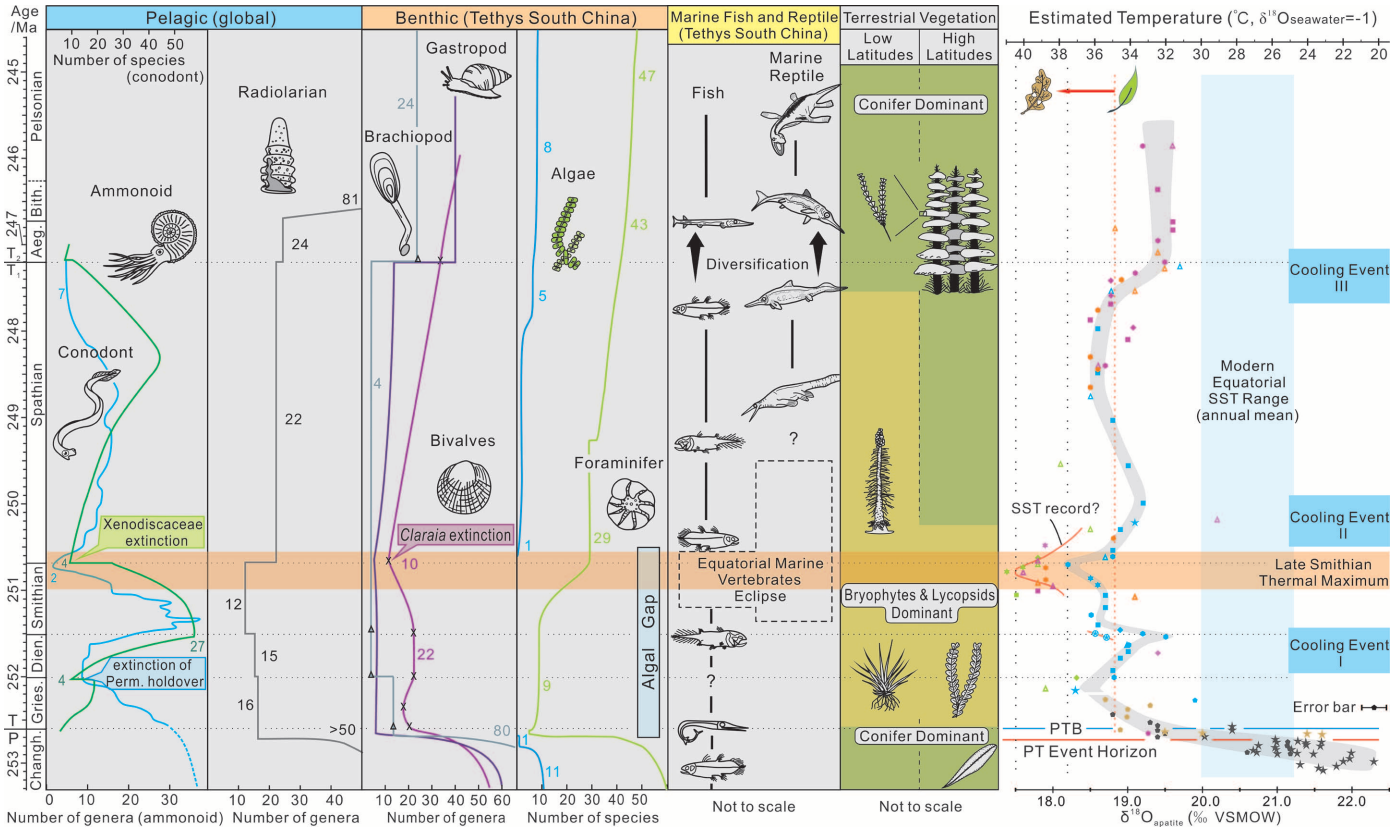

Fig. 3. Early Triassic diversity of major marine groups and temperature trends showing inverse relationship: Peak diversity corresponds to cool climate conditions around the Dienerian-Smithian boundary, early Spathian, and early Anisian (named cooling events I to III), whereas low diversity in Griesbachian and Smithian correlates with peak temperatures. Diversity of marine groups from (*37*–*39*, *49*–*52*); fish and marine reptile only show the general presence of taxa; no quantitative diversity data are available (supplementary text 6). Floral data (*28*–*30*, *42*) show the loss of equatorial conifer-dominated forests above the Permian-Triassic (PT) boundary, with the earlier reappearance of this forest type at high latitudes. Gray band represents the first-order seawater temperatures trend (upper water column, ~70-m water depth) estimated by this study; red trend line represents possible SST derived from shallow water taxa. Same stratigraphic scheme as Fig. 2.

sustainable for short periods (*17*). As a consequence, marine animals cannot long survive temperatures above 35°C, particularly those with a high performance and high oxygen demand, such as cephalopods (*16*).

Extreme equatorial warmth should have left a distinct signature in the Early Triassic fossil records, a proposition that we examine here. The fossil fish record is exceptionally good in the Early Triassic, with many well-preserved faunas known from locations such as Madagascar, Greenland, and British Columbia (supplementary text 6). This is related to the widespread distribution of anoxic facies (*18*) that provide excellent preservational conditions for such fossils. However, our compilation of fish occurrences reveals that they are very rare in equatorial locales, especially during the late Griesbachian and the Smithian, despite being common at higher latitudes at these times (fig. S1 and table S2). This rarity is extraordinary because Early Triassic units, such as the dysoxic-anoxic Daye Formation of South China, are widespread (supplementary text 7) and yet do not yield a fossil fish fauna. The general absence of ichthyofauna in equatorial regions coincides with the temperature maxima reconstructed from the $\delta^{18}O_{apatite}$ record, and we interpret this coincidence as recording equatorial exclusion because of inhospitably high temperatures. In contrast, invertebrates remain common in these intervals (*19*), especially sessile mollusks with their better adapted oxyconforming metabolism allowing them to cope with synergistic stresses of high temperature and low oxygen (*17*, *20*). Like fish, marine reptiles also exhibit high aerobic activity and are likely to have had a relatively low oxygen-limited thermal tolerance. Examining Early Triassic marine reptile (ichthyosaur) occurrences reveals that they too are not found in equatorial waters until the middle-late Spathian (supplementary text 6), ~1 to 2 My after their first appearance in higher latitudes during the Smithian (*21*, *22*). Other notable absences from equatorial oceans are calcareous algae, whose outage spans the entire end-Permian–early Spathian interval although they are present in higher latitudes [e.g., Spitsbergen, (*23*)]. Their equatorial absence (supplementary text 8) likely reflects inhibiting temperatures, whereas the abundance of calcimicrobial carbonates in shelf waters, one of the stand-out features of the Early Triassic (*24*), was possible because of the much higher temperature tolerance of cyanobacterial photosynthesis (*16*).

Critically high temperatures may also have excluded terrestrial animal life from equatorial Pangea, and with SSTs approaching 40°C the land temperatures are likely to have fluctuated to even higher levels. Our compilation of tetrapod fossil occurrences reveals them to be generally absent between 30°N and 40°S in the Early Triassic (Fig. 1), with rare exceptions (*25*, *26*); this is a stark contrast to Middle and Late Triassic occurrences, when they occur at all latitudes (fig. S1). This equatorial "tetrapod gap" does not reflect an absence of suitable strata for their preservation. For example, the Buntsandstein of Europe is one of the best known and most intensively investigated terrestrial formations of the Early Triassic; tetrapods are exceptionally rare in the lower part (Induan) and only become common in middle and upper units (late Early Triassic to Middle Triassic) (*27*). The tetrapod gap of equatorial Pangea coincides with an end-Permian to Middle Triassic global "coal gap" that indicates the loss of peat swamps (*5*). Peat formation, a product of high plant productivity, was only reestablished in the Anisian and then only in high southern latitudes (*5*), although gymnosperm forests appeared earlier (in the Early Spathian), but again only in northern and southern higher latitudes (*28*, *29*). In equatorial Pangea, the establishment of conifer-dominated forests was not until the end of the Spathian (*30*), and the first coals at these latitudes did not appear until the Carnian ~15 My after their end-Permian disappearance (*5*). These signals suggest equatorial temperatures exceeded the thermal tolerance for many marine vertebrates at least during two thermal maxima, whereas terrestrial equatorial temperatures were sufficiently severe to suppress plant and animal abundance during most of the Early Triassic.

Thermal tolerance is likely to decrease for organisms with larger body sizes (*31*). Nonlethal effects of temperature increase include smaller adult size, which, in conjunction with increased juvenile mortality at higher temperatures (*32*, *33*), will produce a fossil record dominated by small individuals. This is a well-known phenomenon in the Early Triassic marine fossil record and has been termed the Lilliput effect (*4*). We suggest that this effect is a response to high temperatures and that it should be most clearly seen in equatorial assemblages, especially during the Griesbachian and Smithian thermal maxima. This prediction is confirmed by data from equatorial marine fossils where small body and trace fossil assemblages are confined to these intervals (*34*, *35*). Low oxygen levels also are known to cause small size in marine invertebrates (*36*), but, although marine dysoxia was a global phenomenon in the Early Triassic (*18*), the restriction of the Lilliput effect to equatorial latitudes indicates that this was primarily a temperature-controlled phenomenon.

The relation between global warming and extinction can be examined in the Early Triassic. The rapid temperature rise across the Permian-Triassic boundary coincides with mass extinction, although absolute temperatures at the time of crisis were only modest [< 30°C (*9*)]. Together with temperature rise, synergistic factors, such as spread of anoxia, may also play important roles in marine extinction (*2*, *18*). However, the subsequent loss of many Permian holdover taxa later in the Griesbachian (conodonts, radiolarian, and brachiopods) may reflect lethal temperatures followed by temporary recovery and radiation in the cooler Dienerian (Fig. 3). The clearest temperature-extinction link is with the LSTM and the end-Smithian event that saw major losses among many marine groups, including bivalves, conodonts, and ammonoids (*37*–*39*). Contemporaneous losses among tetrapods on land (*25*) suggest that this was a crisis that affected a broad diversity of ecosystems.

The ultimate driving factor behind the end-Permian warming long has been attributed to greenhouse gas emissions, either from volcanogenic (*8*) or thermogenic sources (*40*). Both are expected to leave a negative excursion in the $\delta^{13}C$ record, and this is the case for both the end Permian–Griesbachian and Smithian intervals (Fig. 2), although it has yet to be demonstrated that a second pulse of Siberian volcanism occurred in the Smithian. However, to maintain high temperatures for the ~5 My of the Early Triassic requires strong, persistent greenhouse conditions. High temperatures also could greatly enhance the activity of decomposers (e.g., fungi and bacteria), resulting in the release of large amounts of terrestrial light carbon into the atmosphere (*41*) and consequently forming oligotrophic, humus-poor soils as observed in modern Amazon rainforests and in Early Triassic soils of Australia and Antarctica (*42*). Together with global suspension of peat formation, elevated decomposition rates may have led to a significant reduction in organic carbon burial on land further contributing to higher atmospheric CO_2 levels (*43*).

High and oscillating temperatures in the Early Triassic likely controlled the pace and nature of recovery in the aftermath of the end-Permian mass extinction as shown by an inverse relationship between the temperature and biodiversity changes, the temporary loss of both marine and terrestrial vertebrates, and the reduced size of the remaining invertebrates. SSTs derived from $\delta^{18}O$ data offer no evidence that a climate thermostat may ameliorate tropical warming by redistributing warmth to the poles (*44*). Rather, extreme global warming may progressively force taxa to vacate the tropics and move to higher latitudes or become extinct. Marine organisms exhibiting low oxygen-dependent thermal tolerance, such as vertebrates, are the first to leave.

References and Notes

1. M. Bálint *et al.*, *Nat. Clim. Change* **1**, 313 (2011).
2. A. Hallam, P. B. Wignall, *Mass Extinctions and Their Aftermath* (Oxford Univ. Press, Oxford, 1997).
3. J. L. Payne *et al.*, *Science* **305**, 506 (2004).
4. R. J. Twitchett, *Palaeogeogr. Palaeoclimatol. Palaeoecol.* **252**, 132 (2007).
5. G. J. Retallack, J. J. Veevers, R. Morante, *Geol. Soc. Am. Bull.* **108**, 195 (1996).
6. D. L. Kidder, T. R. Worsley, *Palaeogeogr. Palaeoclimatol. Palaeoecol.* **203**, 207 (2004).
7. M. K. Reichow *et al.*, *Earth Planet. Sci. Lett.* **277**, 9 (2009).
8. S. V. Sobolev *et al.*, *Nature* **477**, 312 (2011).
9. M. M. Joachimski *et al.*, *Geology* **40**, 195 (2012).
10. D. L. Clark, W. Cheng-Yuan, C. J. Orth, J. S. Gilmore, *Science* **233**, 984 (1986).
11. Information on materials and methods is available on *Science* Online.
12. T. D. Frank, Data report: Geochemistry of Miocene sediments, Site 1006 and 1007, Leeward margin, Great

Bahama Bank, in *Proceedings of the Ocean Drilling Program, Scientific Results*, P. K. Swart, G. P. Eberli, M. J. Malone, J. F. Sarg, Eds. (Ocean Drilling Program, College Station, TX, 2000), vol. 166, pp. 137–143.
13. J. Berry, O. Bjorkman, *Annu. Rev. Plant Physiol.* **31**, 491 (1980).
14. R. J. Ellis, *Nature* **463**, 164 (2010).
15. G. N. Somero, *Annu. Rev. Physiol.* **57**, 43 (1995).
16. H. O. Pörtner, *Comp. Biochem. Physiol.* **132**, 739 (2002).
17. H. O. Pörtner, *Naturwissenschaften* **88**, 137 (2001).
18. P. B. Wignall, R. J. Twitchett, *Spec. Pap. Geol. Soc. Am.* **356**, 395 (2002).
19. T. Galfetti *et al.*, *Sediment. Geol.* **204**, 36 (2008).
20. H.-O. Pörtner, *J. Exp. Biol.* **213**, 881 (2010).
21. J. M. Callaway, D. B. Brinkman, *Can. J. Earth Sci.* **26**, 1491 (1989).
22. C. B. Cox, D. G. Smith, *Geol. Mag.* **110**, 405 (1973).
23. P. B. Wignall, R. Morante, R. Newton, *Geol. Mag.* **135**, 47 (1998).
24. A. H. Knoll, R. K. Bambach, J. L. Payne, S. Pruss, W. W. Fischer, *Earth Planet. Sci. Lett.* **256**, 295 (2007).
25. S. G. Lucas, *Palaeogeogr. Palaeoclimatol. Palaeoecol.* **143**, 347 (1998).
26. M. Borsuk-Białynicka, E. Cook, S. E. Evans, T. Maryań, *Acta Palaeontol. Pol.* **44**, 167 (1999).
27. H.-D. Sues, N. C. Fraser, *Triassic Life on Land* (Columbia Univ. Press, New York, 2010).
28. T. Galfetti *et al.*, *Geology* **35**, 291 (2007).
29. E. Schneebeli-Hermann *et al.*, *Palaeogeogr. Palaeoclimatol. Palaeoecol.* **339–341**, 12 (2012).
30. C. V. Looy, W. A. Brugman, D. L. Dilcher, H. Visscher, *Proc. Natl. Acad. Sci. U.S.A.* **96**, 13857 (1999).
31. H. O. Pörtner, R. Knust, *Science* **315**, 95 (2007).
32. M. J. Angilletta, *Thermal Adaptation- A Theoretical and Empirical Synthesis* (Oxford Univ. Press, New York, 2009).
33. J. A. Sheridan, D. Bickford, *Nat. Clim. Change* **1**, 401 (2011).
34. B. Metcalfe, R. J. Twitchett, N. Price-Lloyd, *Palaeogeogr. Palaeoclimatol. Palaeoecol.* **308**, 171 (2011).
35. R. J. Twitchett, *Palaeogeogr. Palaeoclimatol. Palaeoecol.* **154**, 27 (1999).
36. G. Chapelle, L. S. Peck, *Nature* **399**, 114 (1999).
37. S. M. Stanley, *Proc. Natl. Acad. Sci. U.S.A.* **106**, 15264 (2009).
38. M. J. Orchard, *Palaeogeogr. Palaeoclimatol. Palaeoecol.* **252**, 93 (2007).
39. J. Chen, in *Mass Extinction and Recovery: Evidences from the Palaeozoic and Triassic of South China*, J. Rong, Z. Fang, Eds. (Univ. of Science and Technology of China Press, Heifei, 2004), vol. II, pp. 647–700.
40. H. Svensen *et al.*, *Earth Planet. Sci. Lett.* **277**, 490 (2009).
41. S. M. Stanley, *Proc. Natl. Acad. Sci. U.S.A.* **107**, 19185 (2010).
42. G. J. Retallack, E. S. Krull, *Aust. J. Earth Sci.* **46**, 785 (1999).
43. W. Broecker, S. Peacock, *Global Biogeochem. Cycles* **13**, 1167 (1999).
44. M. Huber, *Science* **321**, 353 (2008).
45. A. M. Ziegler, M. L. Hulver, D. B. Rowley, in *Late Glacial and Postglacial Environmental Changes–Quaternary, Carboniferous-Permian and Proterozoic*, I. P. Martini, Ed. (Oxford Univ. Press, New York, 1997), pp. 111–146.
46. G. Muttoni *et al.*, *Geoarabia* **14**, 17 (2009).
47. D. J. Lehrmann *et al.*, *Palaios* **18**, 138 (2003).
48. R. A. Locarnini *et al.*, *World Ocean Atlas 2009, Volume 1: Temperature*, S. Levitus, Ed. [National Oceanic and Atmospheric Administration (NOAA) Atlas NESDros. Inf. Serv. 68, U.S. Government Printing Office, Washington, DC, 2010].
49. H. Song *et al.*, *Geology* **39**, 739 (2011).
50. D. Sun, S. Shen, in *Mass Extinction and Recovery: Evidences from the Palaeozoic and Triassic of South China*, J. Rong, Z. Fang, Eds. (Univ. of Science and Technology of China Press, Heifei, China, 2004), vol. II, pp. 543–570.
51. H. Pan, D. H. Erwin, *Palaeoworld* **4**, 249 (1994).
52. L. O'Dogherty *et al.*, *Geodiversitas* **31**, 213 (2009).

Acknowledgments: D. Lutz, F. Nenning, B. Yang, and X. Liu are acknowledged for lab and field assistance. This study was supported by Chinese 973 Program (2011CB808800) and the Natural Science Foundation of China (41172024 and 40830212). Y.S. acknowledges China University of Geosciences and China Scholarship Council for split-site Ph.D. at Wuhan, Leeds, and Erlangen.

Supplementary Materials

www.sciencemag.org/cgi/content/full/338/6105/366/DC1
Materials and Methods
Supplementary Text
Fig. S1
Tables S1 to S4
References (*53*–*150*)

1 May 2012; accepted 4 September 2012
10.1126/science.1224126

A Complete Terrestrial Radiocarbon Record for 11.2 to 52.8 kyr B.P.

Christopher Bronk Ramsey,[1]* Richard A. Staff,[1] Charlotte L. Bryant,[2] Fiona Brock,[1] Hiroyuki Kitagawa,[3] Johannes van der Plicht,[4,5] Gordon Schlolaut,[6] Michael H. Marshall,[7] Achim Brauer,[6] Henry F. Lamb,[7] Rebecca L. Payne,[8] Pavel E. Tarasov,[9] Tsuyoshi Haraguchi,[10] Katsuya Gotanda,[11] Hitoshi Yonenobu,[12] Yusuke Yokoyama,[13] Ryuji Tada,[13] Takeshi Nakagawa[8]

Radiocarbon (^{14}C) provides a way to date material that contains carbon with an age up to ~50,000 years and is also an important tracer of the global carbon cycle. However, the lack of a comprehensive record reflecting atmospheric ^{14}C prior to 12.5 thousand years before the present (kyr B.P.) has limited the application of radiocarbon dating of samples from the Last Glacial period. Here, we report ^{14}C results from Lake Suigetsu, Japan (35°35′N, 135°53′E), which provide a comprehensive record of terrestrial radiocarbon to the present limit of the ^{14}C method. The time scale we present in this work allows direct comparison of Lake Suigetsu paleoclimatic data with other terrestrial climatic records and gives information on the connection between global atmospheric and regional marine radiocarbon levels.

Lake Suigetsu contains annually laminated sediments that preserve both paleoclimate proxies and terrestrial plant macrofossils that are suitable for radiocarbon dating. The lake's potential to provide an important archive of atmospheric radiocarbon (^{14}C) was realized in 1993 (*1*). However, the single SG93 sediment core then recovered included missing intervals between successive sections (*2*). This, together with the difficulty of visual varve counting, resulted in inconsistency between the SG93 and other ^{14}C calibration records (*3*). The SG06 core-set recovered in 2006 consists of four parallel cores that together avoid any such sedimentary gaps (*4*). Here, we report 651 ^{14}C measurements covering the period between 11.2 and 52.8 thousand years before the present (kyr B.P.) tied to a time scale derived from varve counting and temporal constraints from other records. Using visual markers, we applied a composite depth (CD) scale to all cores, including SG93. We also define an event-free depth (EFD), which is the CD with substantial macroscopic event layers (such as turbidites and tephras) removed.

Accelerator mass spectrometry radiocarbon dating (*5*) has been conducted on terrestrial plant macrofossils selected from the SG06 cores to cover the full ^{14}C time range, from the present to the detection limit of the ^{14}C method (0 to 41 m CD) (table S1). The results already reported from the control period (0 to 12.2 kyr B.P.) (*6*), covered by the tree-ring–derived calibration curve (*7*), act to demonstrate the integrity of the sediments and to anchor the floating SG06 varve chronology, because varves do not extend into the Holocene.

The varve-based chronology for SG06 (*5*, *8*, *9*) provides our best estimate of the true age of the cores for the period ~10.2 to 40.0 kyr B.P., based only on information from the site. It provides good relative chronological precision and has the advantage of being independent of other dating techniques. However, the cumulative counting uncertainty inevitably increases with age (~6% at 40 kyr B.P.). The full varve chronology (Fig. 1A and table S1) has been extrapolated on the basis of EFD to cover the period 40 to 53 kyr B.P.

To better constrain the uncertainties in the varve chronology, we can directly compare the Suigetsu data set and other archives that provide information on atmospheric ^{14}C and associated independent ages. The two most useful records for this purpose are the Bahamas speleothem GB89-25-3 (*10*) and the Hulu Cave speleothem H82 (*11*), both of which have extensive ^{14}C- and U-Th–based chronologies. In both cases, we would expect the radiocarbon in the speleothems to respond to changes in atmospheric ^{14}C content, despite the groundwater containing a dead-carbon fraction (DCF) from dissolved carbonates. Estimated DCF for these speleothems was 2075 ± 270 radiocarbon

[1]University of Oxford, Oxford, UK. [2]Natural Environment Research Council Radiocarbon Facility, Scottish Universities Environmental Research Centre, East Kilbride, UK. [3]Nagoya University, Nagoya, Japan. [4]University of Groningen, Groningen, Netherlands. [5]University of Leiden, Leiden, Netherlands. [6]GeoForschungsZentrum German Research Centre for Geosciences, Potsdam, Germany. [7]Aberystwyth University, Aberystwyth, UK. [8]University of Newcastle, Newcastle upon Tyne, UK. [9]Free University Berlin, Berlin, Germany. [10]Osaka City University, Osaka, Japan. [11]Chiba University of Commerce, Chiba, Japan. [12]Naruto University of Education, Naruto, Japan. [13]University of Tokyo, Tokyo, Japan.

*To whom correspondence should be addressed. E-mail: christopher.ramsey@rlaha.ox.ac.uk